Nonlinear analyses of periodic and chaotic time series from the peroxidase-oxidase reaction

ARTICLE *in* THE JOURNAL OF PHYSICAL CHEMISTRY · AUGUST 1993

Impact Factor: 2.78 · DOI: 10.1021/j100134a012

Nonlinear Analyses of Periodic and Chaotic Time Series from the Peroxidase–Oxidase Reaction

Torben Geest,[†,‡] Lars F. Olsen,[*,†,§] Curtis G. Steinmetz,[‡] Raima Larter,[‡] and William M. Schaffer[§]

Physical Biochemistry Group, Institute of Biochemistry, Odense University, Campusvej 55, DK-5230 Odense M, Denmark, Department of Chemistry, Indiana University–Purdue University at Indianapolis (IUPUI), Indianapolis, Indiana 46202, and Department of Ecology and Evolutionary Biology, University of Arizona, Tucson, Arizona 85721

Received: March 10, 1993; In Final Form: May 18, 1993

Experimental time series of $[O_2]$ generated by the peroxidase–oxidase reaction were analyzed using various methods from nonlinear dynamics. The following results were obtained: (1) Aperiodic time series are chaotic as evidenced by (i) the observation of period doubling bifurcations in response to increasing the amount of 2,4-dichlorophenol in the reaction mixture, (ii) well-defined next amplitude maps, (iii) positive Lyapunov exponents corresponding to about 0.5 bits per orbital excursion, and (iv) fractal dimensions ranging from 2.6 to 2.8. Prediction profiles obtained by subjecting the data to nonlinear forecasting give further evidence of deterministic chaos. (2) The chaotic data are nonuniform, since none of the above-mentioned methods work well when applied to the continuous data. Instead, one has to use a series of maxima. (3) Conclusions 1 and 2 are supported by the fact that similar results obtain for chaotic time series generated by a simple model of the reaction.

1. Introduction

In recent years, it has become increasingly apparent that the phenomenon now called *chaos* plays an important role in the overall functioning of living systems.[1–4] Chaotic dynamics have been observed at all levels of the biological hierarchy: at the biochemical level in enzyme reactions;[5,6] at the organismal level, in physiological function and so-called "dynamical diseases";[7] and at the level of whole populations and the diseases that afflict their members.[2] Interestingly, chaos is often associated with "healthy" system behavior, and the loss of chaos with pathology. For example, certain neurological and cardiac anomalies involve reductions in dynamic complexity as evidenced, for example, by EEG and EKG recordings.[8,9] At the population level, theoretical studies[10] suggest that chaos reduces species extinction rates even enhancing the severity of fluctuations in local populations.

The diagnostic property of chaotic dynamics is sensitive dependence on initial conditions (SDIC).[11] Mathematically, this means that nearby trajectories in the phase space on average diverge from each other exponentially. Rates of trajectorial separation are determined by the system's positive Lyapunov characteristic exponents (LCEs).[12,13] Typically, the exponents are defined so that positive values correspond to orbital divergence and negative values to convergence. From this definition, it follows that a chaotic system is one in which there is at least one positive LCE, *i.e.*, there is at least one direction in the phase space in which neighboring orbits diverge. The experimental consequence of SDIC is that the long-term behavior of chaotic systems cannot be predicted save in a statistical sense. More precisely, given the inevitable imprecision in characterizing a system's initial state, it is impossible to predict far into the future other than to assert that there is a limiting probability distribution according to which the system's state will be specified. The latter is sometimes referred to as the system's "invariant measure",[14] and in this sense chaos resembles a random process,[15,16] even though the equations of motion are entirely deterministic. Chaotic dynamics are often manifestly aperiodic with little or no apparent recurrence, but this is not always the case;[17] *i.e.*, chaos can manifest itself as subtle deviations from strict periodicity, in which case the phenomenon is difficult to distinguish from periodic behavior in the presence of noise.

The traditional approach to demonstrate chaos in experimental data has been to look for its so-called "field-marks". In addition to the largest LCE, one can also estimate the Kolmogorov entropy, which gives a bound on the sum of the positive exponents.[14] In principle, positive exponents and entropies indicate the that the dynamics are chaotic. Conversely, if the largest exponent is 0, one may conclude that the dynamics are periodic. Another indicator of dynamical complexity is the system's fractal dimension[18] which indicates the number of independent coordinates required to characterize the motion. In the case of "regular" motion, the system's dimension will be a whole number. For example, periodic dynamics correspond to closed curves in the phase space the dimension of which is 1. Similarly, quasiperiodic dynamics correspond to motion on the surface of a torus, the dimension of which equals the number of incommensurate spectral frequencies. For chaotic fluctuations, the system's dimension must exceed 2 and is often noninteger. The observation of a noninteger or "fractal" dimension is consequently taken as evidence of chaotic dynamics. However, it should be pointed out that fractal attractors exist which are not chaotic.[19]

Demonstrating the existence chaos in experimental data can be a difficult undertaking. In the first place, experimental time series are often of limited duration and are inevitably corrupted by dynamical noise, *i.e.*, perturbations induced by fluctuating ambient conditions, and observational error. The effect of noise is to inflate the estimated values of the LCEs as well as the system's apparent dimension at length scales corresponding to the magnitude of the noise. If the latter is small enough, the system's deterministic character can sometimes be detected at length scales above the noise floor. Unfortunately, dynamical quantities such as the LCEs are defined only at small length scales. Consequently, if the noise amplitude is at all large, one's ability to obtain meaningful estimates of these quantities can be completely compromised.

A second problem, which crops up repeatedly in biological systems, is nonuniformity.[20,21] From a theoretical viewpoint, this means that the frequencies with which the system visits different regions of the phase space are highly disparate. Experimentally, one observes time series with multiple time scales. Examples include "irruptive" time series such as certain population cycles,[22]

* Author to whom correspondence should be addressed.
† Odense University.
‡ IUPUI.
§ University of Arizona.

0022-3654/93/2097-8431$04.00/0

and the relaxation behavior observed in chemical oscillators.[23] An emerging lesson of recent attempts to diagnose chaos in univariate time series is that standard methods of characterizing a system's dynamics founder on the shoals of nonuniformity.[20] To see why this is true, even in the absence of noise, consider the problem of estimating the LCEs. The latter are average rates of stretching and contraction over the entire phase space. In a nonuniform system, regions in which nearby trajectories diverge may be visited infrequently relative to those regions in which neighboring orbits evolve together or converge. Imagine a spiky chaotic time series where the data remain close to some constant value, e.g., zero, most of the time, every now and then interrupted by brief outbursts. Here the probability of finding the trajectory near the "pseudo" fixed point is high, and consequently, if the data are limited, one would obtain a negative Lyapunov exponent. Other nonuniform data, e.g., data from relaxation processes, may yield Lyapunov exponents that are too high under similar circumstances.[21] The greater the degree of nonuniformity, the more data will be required to obtain an accurate estimate. In the limit of a data set consisting of delta functions emerging from a constant background, the time series would have to be of infinite duration.

Attempts to estimate the dimension of nonuniform time series are similarly confounded. For example, spiky time series yield dimension estimates close to zero, because, so far as the dimension algorithm was concerned, the system spent most of its time approximating a stable point.

One approach to dealing with this problem is to transform the data so that the degree of nonuniformity is reduced. A naive approach would be to subject the data to a log transformation, but for the problem of estimating the LCEs, this is inadvisable inasmuch as the exponents are invariant under polynomial, but not logarithmic, transformations. An alternative approach is to extract a discrete mapping from the continuous data by taking what is known as "Poincaré section". This entails recording the points at which continuous orbits intersect an appropriately chosen "slicing plane". Theory tells us that quantitative measures of the system's behavior obtained from the map are simply related to the corresponding measures that obtain from the continuous data.

The case for chaos can sometimes be buttressed in two additional ways. In the first instance it may be possible to induce a succession of dynamical states by varying the ambient circumstances, for example, by varying the temperature or the concentration of a reactant. If the resulting bifurcation corresponds to one of the established "routes to chaos" such as period-doubling,[24,25] one gains additional confidence that the apparently aperiodic oscillations one observes experimentally are, in fact, chaotic and not simply some mixture of periodicity and noise.

A second way of strengthening one's conclusions entails the use of mathematical models. In the case that one can write down equations that accurately describe the observed behavior, one can use the simulated output as a test signal for the algorithms used to estimate dynamical quantities from the single valued time series. This allows one to control for algorithmic failure in the face of factors such as nonuniformity.

In the present paper, we study periodic and chaotic fluctuations in the peroxidase–oxidase reaction. The peroxidase–oxidase reaction entails the reduction of molecular oxygen with reduced nicotinamide adenine dinucleotide as the electron donor:

$$O_2 + 2NADH + 2H^+ \rightarrow 2H_2O + 2NAD^+ \qquad (1)$$

When the reaction takes place at low pH with continuous supplies of NADH and O_2 and in the presence of 2,4-dichlorophenol and methylene blue, the concentrations of O_2, NADH, and the enzyme intermediate compound III oscillate.[26-29] Depending on the experimental conditions, these oscillations may be periodic, quasiperiodic or chaotic.[5,30-35] Recently a period-doubling route to chaos was established experimentally by increasing the concentration of dichlorophenol in the reaction mixture.[32]

2. Materials and Methods

2.1. Experimental Procedures. The experiments were conducted in a 20 mm × 20 mm quartz cuvette fitted with a stirrer. The cuvette was mounted in an Aminco DW2000 spectrophotometer. O_2 was supplied to the reaction mixture from a head space above the liquid; the oxygen content of the gas phase was controlled by mixing oxygen and nitrogen using a gas mixer constructed in our workshop. The oxygen content of the gas phase was in the range 1.42% (v/v). The rate of transport of oxygen into the liquid, v_T, is given by[36]

$$v_T = K([O_2]_{eq} - [O_2]) \qquad (2)$$

where K is a constant that depends on the area of the gas–liquid interface and hence on the stirring rate. $[O_2]$ is the oxygen concentration in the liquid and $[O_2]_{eq}$ is the concentration at equilibrium between the liquid and the gas. In the present experiments, K was measured as 0.0037 s^{-1}. A concentrated solution (0.08–0.20 M) of NADH was pumped into the liquid at a constant rate of 20–40 μL/h using syringe pumps from Harvard Apparatus and Sage Instruments. O_2 was measured using a Radiometer oxygen electrode; NADH was measured spectrophotometrically by subtracting the absorbances at 360 and 380 nm. The reaction mixture (7 mL) contained 0.1 M acetate buffer, pH 5.1, 15–40 μM, 2,4-dichlorophenol, 0.1 μM methylene blue, and 0.5–1.0 μM peroxidase. The temperature was 28 °C. NADH and peroxidase (RZ 3.0) were obtained from Boehringer. The data from the spectrophotometer and the oxygen electrode were both sampled at 1-s intervals by a personal computer through an interface board and stored on disk for later analyses.

2.2. State Space Reconstruction from Experimental Data. To analyze our experimental data we generated a pseudophase space using the so-called "method of delays".[37] Here, one chooses a time delay, T, and, if $y(t)$ is an observable, constructs the flow of $y(t)$, $y(t+T)$, $y(t+2T)$, ..., $y(t+(m-1)T)$. From the reconstructed flow we then constructed Poincaré sections[38,39] and "return maps" which specify the sequence in which points on the section are visited. Analogous to computing such a map is to record successive maxima in the experimental time series. This amounts to slicing the reconstructed flow with a surface that passes through all of the maxima in the observable.[40] In the simple case of flows of dimension <3, such "next maximum" or "next amplitude" maps, as they are called, encapsulate recurrence relations of the form

$$Z_i = F(Z_{i-1}, Z_{i-2}) \qquad (3)$$

where Z_i is the ith maximum in the observable. For nonuniform systems, the sequence of successive maxima often yields better estimates of the dynamical quantities than the flow from which they are extracted (see the preceding discussion).

2.3. Estimating Dynamical Quantities from the Data. For experimental time series, it is practical to estimate the largest LCE, λ_1, and D_2, the so-called correlation dimension. For the former, we use the "fixed evolution time" method proposed by Wolf *et al.*,[13] while for the latter we adopt the procedure described by Grassberger and Procaccia.[43] The latter is calculated by estimating the correlation integral, $C(g)$, defined as

$$C(g) = \lim_{N\to\infty} (1/N^2) \sum_{i \neq j} H(g - |X_i - X_j|) \qquad (4)$$

Here H is the Heaviside function and X_i and X_j are points on the attractor. $C(g)$ counts the number of point pairs whose distance is smaller than g. It can be shown that $C(g)$ scales as

$$\ln C(g) \sim D_2 \ln g \qquad (5)$$

Note that D_2 gives a *lower* bound on the "information dimension,"

D_I, which is what one usually means by the term "fractal dimension".[18] These computations can be performed on both the experimental flows and the sequences of successive maxima obtained therefrom. Lyapunov exponents are often measured in bits per unit time. Thus, if $\lambda_{1,flow}$ is the largest Lyapunov exponent calculated for the continuous data and $\lambda_{1,map}$ is the exponent calculated from the discrete sequence of maxima we expect

$$\lambda_{1,flow} = \lambda_{1,map}/\tau \tag{6}$$

where τ is the average time interval between maxima. For the dimensions we expect

$$D_{2,flow} = D_{2,map} + 1 \tag{7}$$

Equations 6 and 7 are valid for uniform time series. For nonuniform data, we expect that analyses of the flow will either *over*estimate or *under*estimate the maximum LCE and *under*estimate the dimension.

An alternative procedure for estimating the maximum Lyapunov exponent from the data entails the use of a recently developed methodology called "nonlinear forecasting".[44,45] Here, one attempts to predict the time evolution of a chaotic data set by inducing one or more relationships, called "predictors," that describe the system's time evolution over various time intervals. Various predictors can be used (see below), but the essential points are first that predictability declines with the length of the forecasting interval, T_p, and second that the maximum LCE and the Kolmogorov entropy can be related to the rate at which forecasting efficacy declines. With regard to the second point, two methods have been proposed.

The first method is due to Farmer and Sidorowich[46] and involves calculation of the normalized root-mean square error:

$$\langle E^2 \rangle = \frac{\langle (x_i - y_i)^2 \rangle}{\langle (y_{i-T_p} - \langle y_{i-T_p} \rangle)^2 \rangle} \tag{8}$$

Here x_i and y_i denote the predicted and the observed values of x at time i, respectively, and the angle brackets denote the average values. Farmer and Sidorowich showed that log (E) scales as

$$\log (E) \sim \lambda_1 T_p \tag{9}$$

The second method is due to Wales.[47] In this case, one calculates the quantity

$$\gamma = \left[\frac{2\langle y_i^2 \rangle}{\langle x_i^2 \rangle + \langle y_i^2 \rangle - 2\langle x_i \rangle \langle y_i \rangle - 2r\sigma(x_i)\sigma(y_i)} \right]^{1/2} - 1 \tag{10}$$

where $\sigma(x_i)$ and $\sigma(y_i)$ are the variances of the distributions $\{x_i\}$ and $\{y_i\}$, respectively, and r is the correlation coefficient. Wales showed that log (γ) scales as

$$\log (\gamma) \sim -KT_p \tag{11}$$

where K is the Kolmogorov entropy. The latter gives an upper bound on the sum of the positive LCEs, and, in the case of systems for which there is only one positive exponent, on the maximum LCE. Again, the calculation can be performed either on the original experimental time series or on the sequence of maxima.

2.4. Estimating Dynamical Quantities from Models. The methods of the preceding section can also be applied to the output of mathematical models. As noted above, if one has a good model, such calculations can serve as a check on the efficacy of one's algorithms. In addition, one can obtain independent estimates. With regard to the maximum LCE, one can compute the entire spectrum of exponents directly from the equations. From this computation, one can further estimate the so-called Lyapunov dimension, D_L. Specifically, D_L is defined by the relation

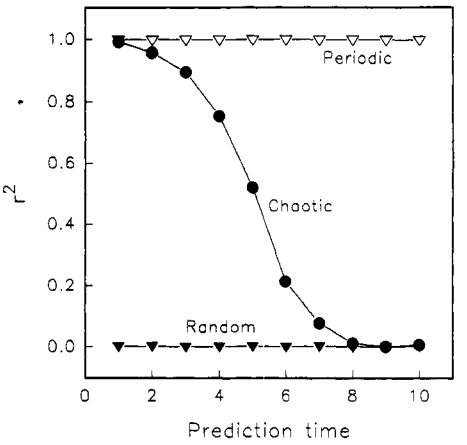

Figure 1. Nonlinear forecasting of a periodic time series, a chaotic time series, and a random time series. The squared correlation coefficient between observed and predicted values, r^2, is plotted against the prediction time T_p. The three time series are discrete and the unit for T_p is therefore *iterations*. Note that for the periodic time series r^2 is always close to 1 irrespective of the magnitude of T_p, whereas for the random time series r^2 remains close to zero. For the chaotic time series, however, r^2 starts out close to 1 for small prediction times, but declines toward zero as T_p is increased.

$$D_L = j + \frac{\lambda_1 + \lambda_2 + \ldots + \lambda_j}{-\lambda_{j+1}} \tag{12}$$

where $\{\lambda_1, \lambda_2, \ldots, \lambda_N\}$ is the complete spectrum of LCEs and j is the maximum integer for which $\lambda_1 + \lambda_2 + \ldots + \lambda_j \geq 0$.[18] For chaotic systems, D_L, gives an upper bound for the fractal dimension, D_I. Thus we have

$$D_2 \leq D_I \leq D_L$$

In the case of uniform systems, $D_2 = D_L$. Otherwise D_2 is strictly less than D_L, in which case, the disparity between the two dimensions gives a measure of the degree of nonuniformity.

2.5. Nonlinear Forecasting as a Method for Distinguishing Chaos from Periodicity plus Noise. It is now widely recognized[48,49] that the algorithms used to estimate LCEs and dimensions can be "fooled" by stochastic data in which there is periodicity, but no chaos. One attempt to distinguish chaos from periodic behavior in the presence of observational noise is due to Sugihara and May.[45] Here one studies the decline in forecasting efficacy of an experimental data set under nonlinear forecasting. Typically, one divides a time series into two parts. The first portion, the so-called "atlas" is then used to induce predictors that describe the time evolution of points in a reconstructed state space over various intervals. The efficacy of the predictors is then assessed by using them to generate forecasts for the second portion of the time series, which is sometimes referred to as the "target data." Nonlinear forecasting thus replaces the problem of extrapolating a time series with that of interpolating a phase portrait. The predictors, themselves come in various forms. Following Farmer and Sidorowich,[44] Sugihara and May used local maps of zeroth order.[50]

Sugihara and May's contribution to this discussion was to point out that the prediction profiles (Figure 1) for periodic data in the presence of observational error and chaotic data are quite different. In the first instance, predictability depends only on the noise level and is essentially independent of the forecasting interval, whereas for chaotic data, forecasting efficacy declines as a consequence of SDIC. In what follows, we apply zeroth-order forecasting algorithm[55] similar to those used by Farmer and Sidorowich[44] and Sugihara and May[45] to both the experimental data and the output of mathematical models.

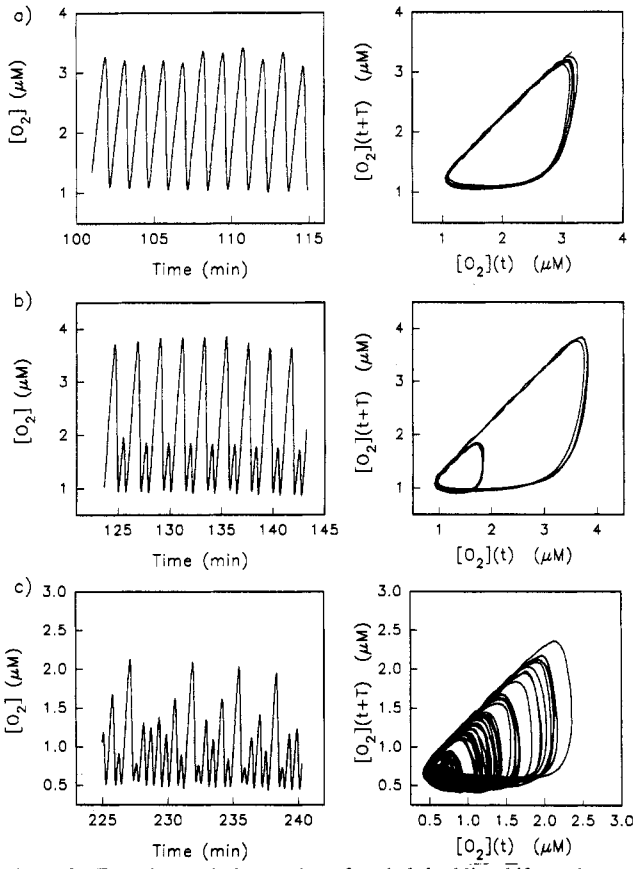

Figure 2. Experimental observation of period doubling bifurcations to chaos in the peroxidase–oxidase reaction. To the left are shown the time series of oxygen. To the right are shown a two-dimensional projection of phase plots of the reconstructed time series using a time delay $T = 6$ s. Experimental conditions were 0.7 μM peroxidase, 0.1 μM methylene blue, and (a) 15 μM dichlorophenol, (b) 20 μM dichlorophenol, and (c) 29 μM dichlorophenol; 0.077 M NADH was infused at a rate of 34 μL/h. Other conditions as described in Materials and Methods.

3. Results and Discussion

3.1. Experimental Data—Lyapunov Exponents and Dimensions. Experimental time series of O_2 and NADH were obtained from the peroxidase-oxidase reaction as discussed in section 2.1. Both periodic and apparently chaotic states were observed. Because the measurements of NADH were insufficiently precise for nonlinear analysis, the following discussion is based entirely on the analysis of O_2 concentrations. Figure 2 shows an example of period-doubling bifurcations of O_2 oscillations obtained by increasing the concentration of dichlorophenol. The transition from simple cycles (Figure 2a) to period-2 oscillations (Figure 2b) to period-4 cycles, *etc.*, and finally to chaos (Figure 2c) is one of the classical bifurcation sequences leading to chaotic dynamics,[24,25] and its observation in the experimental data is perhaps the most compelling evidence that aperiodic fluctuations in this reaction really are the manifestations of a chaotic process. Typical time series (left) and two-dimensional projections of reconstructed phase portraits (right) are given in Figure 2. Figure 3 shows a next-amplitude map obtained from an aperiodic time series. Unlike previously published maps[5,30,31] obtained for the peroxidase–oxidase reaction under slightly different conditions, the map has a single maximum and differs somewhat in its shape.

Figure 4 shows running estimates of the maximum LCE obtained using the FET algorithm[13] for representative periodic and chaotic time series. The data were embedded in 3 or 4 dimensions, with a delay of 6 s. Following Wolf *et al.*[13], the evolution time was set equal to the average period of oscillation

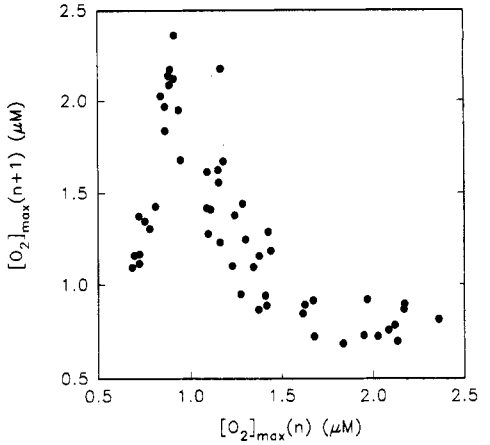

Figure 3. Next-amplitude map constructed by plotting each of the amplitudes of the oscillations of $[O_2]$ from the experiment in Figure 2c against the preceding amplitude.

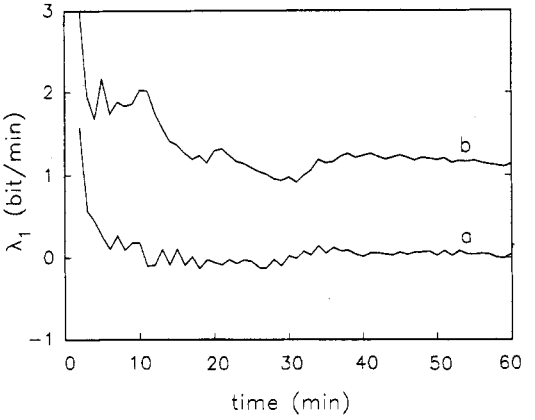

Figure 4. Estimation of the maximum Lyapunov exponent of (a) a periodic oscillation and (b) and aperiodic oscillation of O_2 using the FET algorithm. 3600 data of each time series were embedded in 4 dimensions using a time delay, $T = 6$s. Evolution time was 60 s and the minimum and maximum replacement length scales were 2 and 10% of the maximum signal size respectively. The experimental conditions were (a) 0.95 μM peroxidase, 0.1 μM methylene blue and 20 μM dichlorophenol; 0.08 M NADH was infused at rate of 39 μL/h; (b) 0.7 μM peroxidase, 0.1 μM methylene blue and 35.7 μM dichlorophenol; 0.2 M NADH was infused at rate of 22.5 μL/h. Other conditions as described in Materials and Methods.

which was 1.03 min. For the periodic data, we obtain $\lambda_1 = 0$ bit/min, whereas for the chaotic time series, $\lambda = 1.2$ bits/min. These values are what one expects for periodic and chaotic time series, respectively; *i.e.*, the periodic system yields a maximum LCE of zero, whereas the putatively chaotic time series yields a positive LCE. In order to compare the magnitude of latter with estimates obtained by other methods, we normalize it according to eq 6. This yields a figure of 1.24 bits/excursion. Comparable results were obtained for the other experiments, *i.e.*, for the periodic time series, the maximum exponent was close to zero, whereas for the chaotic data, λ_1 ranged from 1 to 2 bits/excursion. Estimates of D_2 were obtained for both the periodic and chaotic time series as prescribed by Grassberger and Procaccia.[43] The data were successively embedded in dimensions 2–8 using a time delay of 6 s. Correlation integrals, $C(g)$, were estimated according to eq 4. Figure 5 shows the resulting plots of ln $(C(g))$ vs ln (g). The lines indicate the scaling regions used for estimating D_2 itself.[56] For the periodic data (Figure 5a), we obtained a limiting slope (*i.e.*, with increasing dimension) of 1, which is what one expects. For the chaotic data (Figure 5b), the corresponding number is approximately 1.5, and for the remaining chaotic time series ranged from 1.2 to 1.5. These values are too low,[58] inasmuch as continuous chaos requires a minimum dimension in excess of 2. Our estimate for D_2 thus suggests that the aperiodic data are nonuniform. As shown in Figure 6, three-dimensional recon-

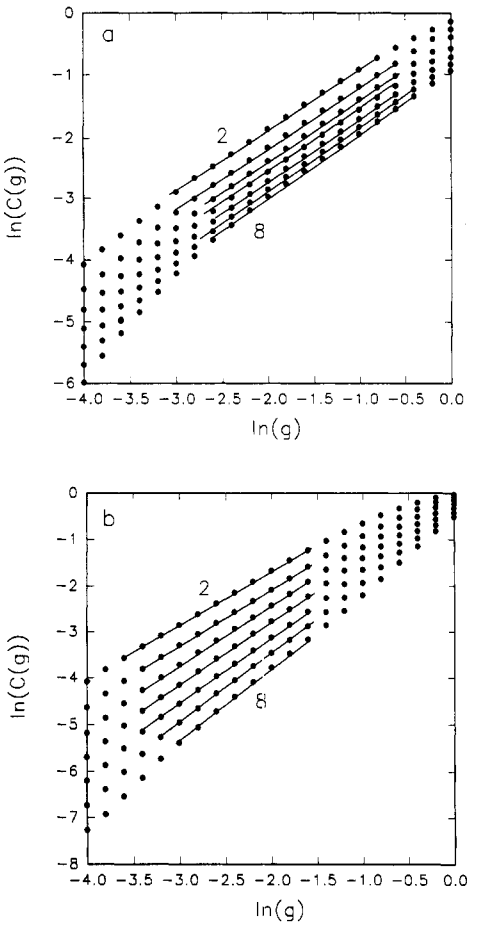

Figure 5. Double logarithmic plots of the correlation integral, $C(g)$, versus length scale, g, for (a) a periodic oscillation and (b) an aperiodic oscillation of O_2. 3600 data were embedded in dimensions 2–8 using a time delay, T = 6s. Experimental conditions as in Figure 4.

structions of the data are consistent with this conjecture, *i.e.*, the majority of points are concentrated in a thick "bundle" indicated by the arrow. These points represent the near-exponential rise in oxygen after the reaction has terminated[28] and hence are highly correlated. Note, however, that the reconstructions in Figure 6 say nothing about how the data are unfolded by higher dimensional embeddings.

Albano *et al.*[59] have pointed out that estimates of D_2 may be sensitive to the sampling interval; *i.e.*, if time between data determinations is too short, surprisingly low values of D_2 may result. Nonuniform data are especially sensitive to this problem compared to their uniform counterparts. However, as noted above, reliable dimension estimates can often be obtained from Poincaré sections even in the presence of nonuniformity.[60] Since the dimension of a Poincaré section is the dimension of the flow *minus* one (eq 7) we must add one to the value obtained in order to get the dimension of the corresponding flow. An easy way to obtain a Poincaré section is to compute the maxima of the corresponding continuous time series.[61] We therefore obtained five time series of maxima of $[O_2]$ from the corresponding irregular time series. The results of our analysis are summarized in Table I. A double logarithmic plot of correlation integral vs length scale for one of these data sets is shown in Figure 7. For one of the time series, there was no saturation of slope with increasing embedding dimension and D_2 could not be estimated. For the remaining data sets, the slopes did converge and D_2 ranged from about 1.6 to 1.8. Note that since time series of maxima are effectively Poincaré sections, the dimensions of the corresponding flows range from 2.6 to 2.8. Unlike the estimates obtained from the flows themselves, these numbers are consistent with the hypothesis of continuous chaos.

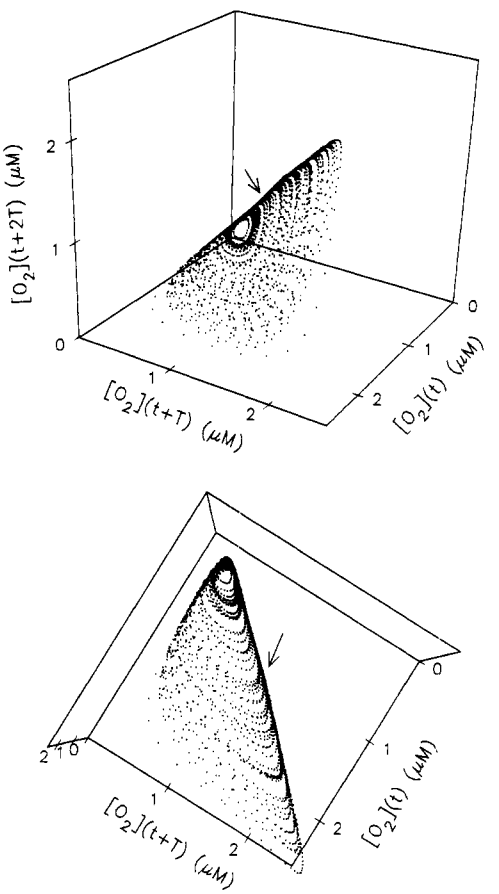

Figure 6. Three-dimensional flow of an aperiodic oscillation of O_2. 3600 data were reconstructed in three dimensions using a time delay, T = 6s. Experimental conditions as in Figure 4b.

TABLE I: Maximum Lyapunov Exponent and Correlation Dimension Computed for Experimental Series of Maxima of O_2[a]

no. of maxima	λ_1	D_2
48	0.63	1.64
57	0.65	*b*
55	0.36	1.70
74	0.48	1.61
59	0.42	1.79

[a] The units of λ_1 are bit/excursion. [b] Slope of ln ($C(g)$) versus ln (g) does not saturate with increasing embedding dimension.

Estimates of λ_1 based on successive maxima are also included in Table I. The values ranged from 0.36 bits/excursion to 0.65 bits/excursion. These numbers are lower than the estimates of 1–2 bits/excursion obtained from the flows. In sum, the next-amplitude maps yielded lower estimates of the maximum exponent and higher estimates of D_2 than the corresponding analyses of the flows. The discrepancies are consistent with the aforementioned hypothesis of nonuniformity. Furthermore, the values obtained for D_2 suggest that the next-amplitude maps may be better suited for nonlinear analysis than the continuous time series.

3.2. Results from Nonlinear Forecasting. We further analyzed the aperiodic time series by subjecting the data to nonlinear forecasting. The results obtained for a representative continuous time series are presented in Figure 8. Here, we display observed *versus* predicted oxygen concentrations for a prediction time of 1 s (Figure 8a) and 10 s (Figure 8b). In the former case, the squared correlation coefficient, r^2, between predicted and observed values is 0.99, whereas in the latter instance, r^2 = 0.29. Figure 8c shows how r^2 varies with the prediction time in the interval $1\text{ s} \leq T_p \leq 40$ s. Note that the initial sigmoidal decline in r^2, is followed by a pronounced rise. This pattern does not conform to either of the alternatives discussed by Sugihara and May,[45]

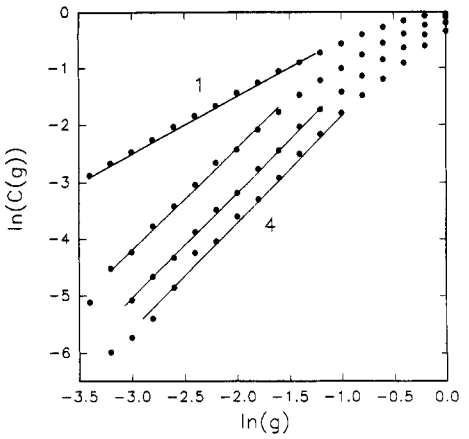

Figure 7. Double logarithmic plots of the correlation integral, $C(g)$, versus length scale, g, computed using the maxima of an aperiodic oscillation of O_2. 59 maxima were embedded in dimensions 1–4 using a delay, T = 1 excursion. Experimental conditions as in Figure 4b.

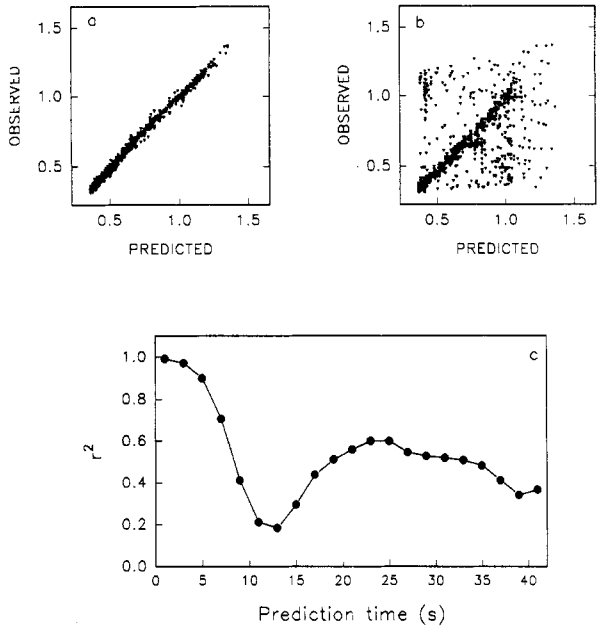

Figure 8. Nonlinear forecasting of an aperiodic oscillation of O_2. In (a) and (b) we have plotted the predicted *versus the observed* values of O_2 for prediction times of 1 and 10 s, respectively. In (c) we have plotted the squared correlation coefficient *versus* the prediction time. 2035 data were embedded in 3 dimensions using a time delay, T = 6s. The first 1000 points were used as an "atlas" to predict the remaining 1035 points. In each prediction only the points within an epsilon ball corresponding to 2% of the maximum signal size were used for the prediction and the maximum number of such points were furthermore limited to 5. Experimental conditions were 0.7 μM peroxidase, 0.1 μM methylene blue, and 32.1 μM dichlorophenol; 0.08 M NADH was infused at rate of 36 μL/h. Other conditions as described in Materials and Methods.

but we have observed[62] similar prediction profiles in chaotic time series with a strong periodic component.[63] In fact, the data analyzed in Figure 8c contain a prominent spectral peak at a frequency corresponding to the oscillation in r^2.

The average period of the data analyzed in Figure 8 was 28 s, and a disturbing aspect of the analysis is that is not possible to make accurate predictions for even a single oscillation. Repeating the computation for the corresponding discrete time series of maxima gives a somewhat different picture. Here (Figure 9a), $r^2 \approx 0.9$ for one-step (28 s) predictions while for four-step predictions (112 s) $r^2 \approx 0.5$. For the continuous data, $r^2 \approx 0.5$ when the prediction time is 8 s.

As noted above (section 2.4), the decline in predictability can be used to provide independent estimates of λ_1. The method proposed by Farmer and Sidorowich[46] entails computation of the

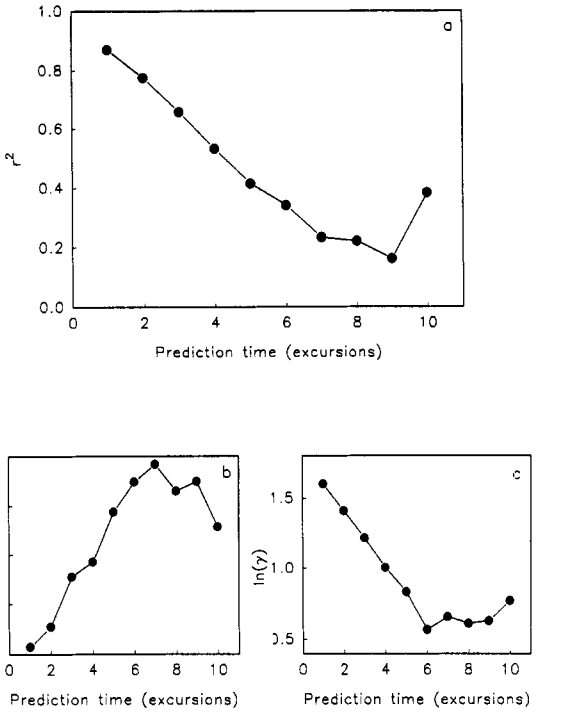

Figure 9. Nonlinear forecasting of the maxima of an aperiodic oscillation of O_2. In (a) we have plotted the squared correlation coefficient *versus* the prediction time. In (b) we have plotted the logarithm of the normalized error defined by eq 8 *versus* the prediction time and in (c) the logarithm of γ defined by eq 10 *versus* the prediction time. 74 maxima were embedded in 2 dimensions using a time delay, T = 1 excursion. The first 37 maxima were used as an atlas to predict the remaining 37 maxima. In each prediction only the nearest 3 points were used. Experimental conditions as in Figure 8.

normalized root mean square error, E. In Figure 9b we plot log (E) *vs* the prediction interval, T_p. The plot is roughly linear up to predictions times corresponding to six excursions and from eq 9, we estimate λ_1 = 0.24 bit/excursion. The method proposed by Wales[47] gives an estimate of the Kolmogorov entropy, K, in terms of the quantity γ, as given by eqs 10 and 11. In Figure 9c, we plot log (γ) *vs* T_p. Again the plot is roughly linear up to six prediction steps, and we obtain an estimate of 0.27 bit/excursion. An alternate procedure suggested by Wales[47] entails plotting the quantity, log ($1 - r$) *vs* T_p. This yields a somewhat higher estimate of 0.43 bit/excursion. These estimates are of the same order of magnitude as those obtained using the method of Wolf *et al.*[13] They are substantially lower than those obtained by applying nonlinear forecasting to the continuous time series. In this case, eqs 8 and 10 yield estimated values of λ_1 of 11.1 bits/excursion and 11.4 bits/excursion respectively. Once again, the disparity of the estimates obtained from the flows and the maps are consistent with the hypothesis of nonuniformity.

4. Models of the Peroxidase–Oxidase Reaction

Essentially two types of models exist for the peroxidase–oxidase reaction: (i) minimal models, which incorporate only the essential features of the reaction[28,30,31] and detailed models, which purport to include all important reaction steps.[66–68] The latter are more difficult to study as they involve the estimation of many rate constants. They are also more computationally intensive. Here we discuss (a) the Olsen 83 model,[30,31] which is an example of a minimal model, and (b) a detailed model proposed by Aguda and Larter[68] to which they refer as model C. The Olsen 83 model involves four chemical species called A, B, X, and Y, where A represents oxygen, B represents NADH, and X and Y represent free-radical intermediates. Model C involves 10 chemical species, five of which are enzyme intermediates.

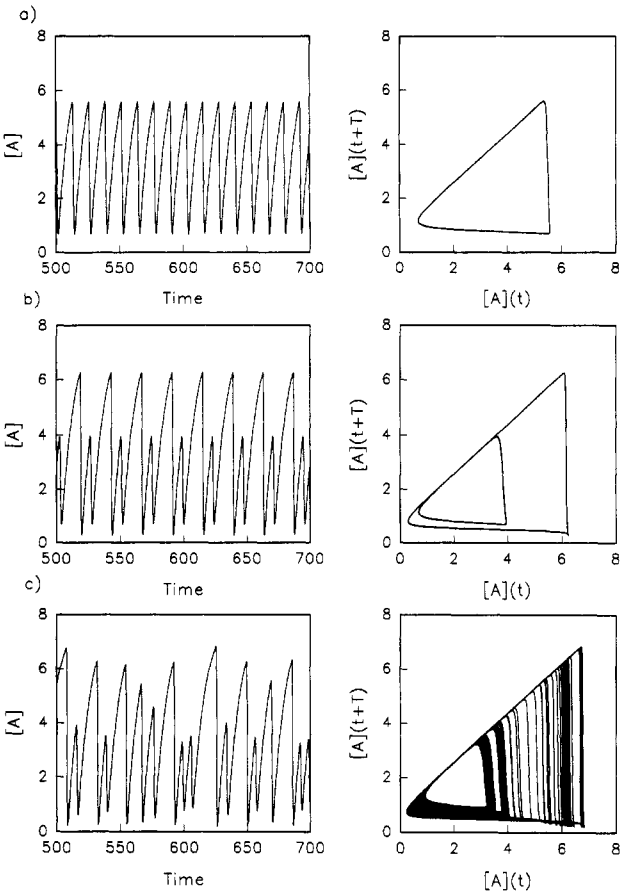

Figure 10. Period doubling bifurcations to chaos in the Olsen 83 model obtained by varying k_3. To the left are shown the time series of A. To the right are shown a two-dimensional projection of phase plots of the reconstructed time series using a time delay $T = 1$ time unit. The values of k_3 are (a) 2.5×10^{-2}, (b) 3.3×10^{-2}, and (c) 3.5×10^{-2}. Other rate constants are $k_1 = 0.35$, $k_2 = 2.5 \times 10^2$, $k_4 = 20.0$, $k_5 = 5.35$, $k_6X_0 = 10^{-5}$, $k_7 = 0.1$, $k_8B_0 = 0.825$, $A_0 = 8.0$. Concentrations of A and rate constants are in dimensionless units.

4.1. The Olsen 83 Model. The Olsen 83 model translates into the following set of first-order differential equations:[30]

$$dA/dt = k_7(A_0 - A) - k_3ABY \quad (13)$$

$$dB/dt = k_8 - k_1BX - k_3ABY \quad (14)$$

$$dX/dt = k_1BX - 2k_2X^2 + 3k_3ABY - k_4X + k_6X_0 \quad (15)$$

$$dY/dt = 2k_2X^2 - k_3ABY - k_5Y \quad (16)$$

Numerical integration of these equations yields a variety of motions depending on the values of the rate constants k_1–k_8. For some values, one obtains regular oscillations, whereas for others the dynamics are chaotic. The transition from simple periodic motion to chaos is illustrated in Figure 10. Here we plot representative time series and two-dimensional reconstructions of the dynamics for increasing values of k_3. It can be argued that changing k_3 is analogous to changing the concentration of dichlorophenol in the experiments[69] and comparison of Figure 10 and 2 reveals striking similarities. In particular, we note that both the model and the experimental data evidence a transition to chaos via period-doubling. Additional simularities can be observed by comparing the bifurcation diagrams.[69] On the other hand, the next-amplitude map (Figure 11) of the simulated reaction appears to differ from the corresponding map computed from the data by virtue of its broad maximum and obvious fractal structure.[30]

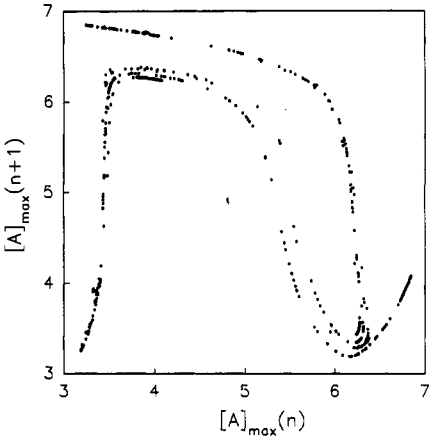

Figure 11. Next-amplitude map of the aperiodic oscillations in Figure 10c.

TABLE II: The Three Largest Lyapunov Exponents and Lyapunov Dimensions for the Peroxidase–Oxidase Model[a]

k_3	λ_1	λ_2	λ_3	D_L
0.025	0.000	–0.69	–0.72	1.00
0.033	0.000	–0.05	–1.40	1.00
0.034	0.447	0.00	–1.93	2.23
0.035	0.444	0.00	–2.99	2.15
0.036	0.361	0.00	–3.62	2.10

[a] The exponents are normalized to the average period of oscillation and are therefore expressed in units of bit/excursion.

TABLE III: Maximum Lyapunov Exponents and Correlation Dimensions Computed from 500 Maxima of A at Various Values of k_3

k_3	λ_1	D_2
0.025	0.01 ± 0.01	0.00 ± 0.00
0.033	–0.02 ± 0.02	0.00 ● 0.00
0.034	0.54 ± 0.02	1.25 ± 0.03
0.035	0.44 ± 0.01	1.04 ● 0.02
0.036	0.41 ± 0.03	1.02 ± 0.02

As noted above, one can estimate the complete spectrum of LCEs for a mathematical model using the procedure described by Benettin *et al.*[12] and Wolf *et al.*[13] The first three exponents are listed in Table II for different values of k_3 together with the corresponding Lyapunov dimension computed from eq 12. Note that, when $k_3 \geq 0.034$, *i.e.*, when the dynamics are chaotic, λ_1 is positive and D_L is slightly larger than 2, *i.e.*, noninteger.

The foregoing estimates can be compared with those obtained by treating the output, *i.e.*, the time series $A(t)$, of the model in the same way that we analyzed the experimental data. Proceeding in this fashion for the flows yields $\lambda_1 = 0$ bits/excursion for the k_3 values corresponding to Figure 10, a and b (periodic behavior) and $\lambda_1 = 2.8$ bits/excursion for the k_3 value corresponding to Figure 10c (chaos). Note that while the first two numbers are correct, the estimate obtained from the chaotic time series is off by a factor of 6–7. Similar results obtain when D_2 is estimated from the simulated data; *i.e.*, the estimates for all three times series are close to 1. In sum, application of conventional algorithms to the simulated flow yields reasonable estimates of λ_1 and D_2 for periodic motions in the Olsen 83 model and unreasonable estimates for chaotic motions. Thus, the problems associated with nonuniformity in the experimental data are also relevant to the model and apparently to an even greater degree.

In the case of the experimental data, switching from the continuous time series to next amplitude maps gave noticeable improvements in D_2 and lower values of λ_1. Table III lists estimates of λ_1 and D_2 computed for sequences of 500 maxima. For all parameter values, the exponents computed from maxima are close to the corresponding values given in Table II. Moreover, the values of $D_2 + 1$ are comparable to but smaller than the

TABLE IV: Effect of the Number of Maxima on the Estimates of λ_1 and D_2 in the Peroxidase–Oxidase Model (k_3 = 0.035)

no. of maxima of A	λ_1	D_2
50	0.61 ± 0.07	1.15 ± 0.10
500	0.41 ± 0.02	1.04 ± 0.01
5000	0.44 ± 0.02	1.03 ± 0.03

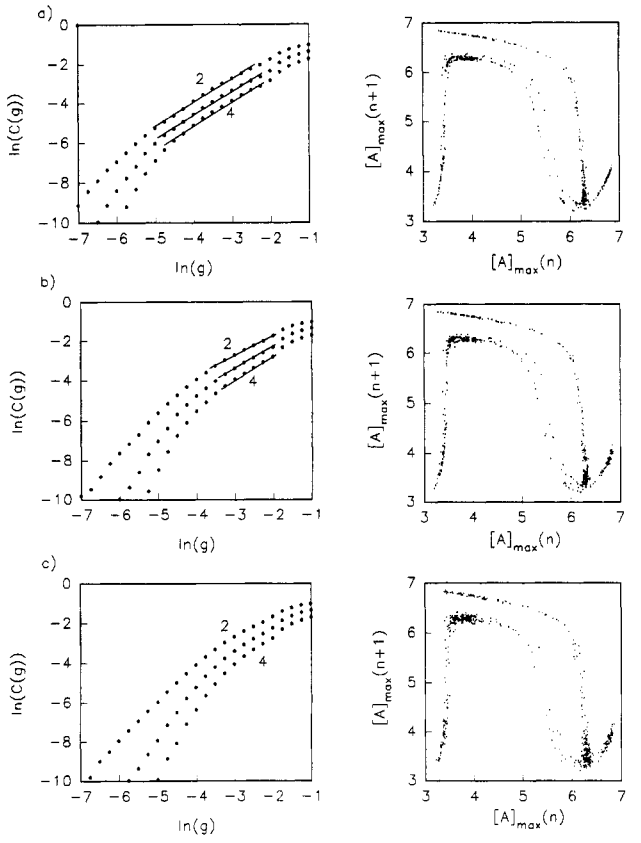

Figure 12. Effect of noise on the correlation integral and next-amplitude plots. Double logarithmic plots of correlation integral versus length scale (left) and next-amplitude plots (right) for 500 maxima of A in the peroxidase–oxidase model. Uniform noise in the interval (a) ±.005, (b) ±0.01, and (c) ±0.02 was added to B 50 times per time unit, $k_3 = 3.4 \times 10^{-2}$. Other rate constants as in Figure 10.

TABLE V: Effect of Noise on the Estimates of λ_1 and D_2 in the Peroxidase–Oxidase Model (k_3 = 0.034)[a]

σ[b]	λ_1	D_2
0.005	0.46 ± 0.06	1.32 ± 0.07
0.01	0.45 ± 0.04	[c]
0.02	0.47 ± 0.09	

[a] 500 maxima of A were used for the calculations. [b] Uniform noise in the interval $\pm\sigma$ is added to B 50 times per time unit. [c] Indicates that the slope of the plot ln ($C(g)$) versus ln (g) does not saturate with increasing embedding dimension.

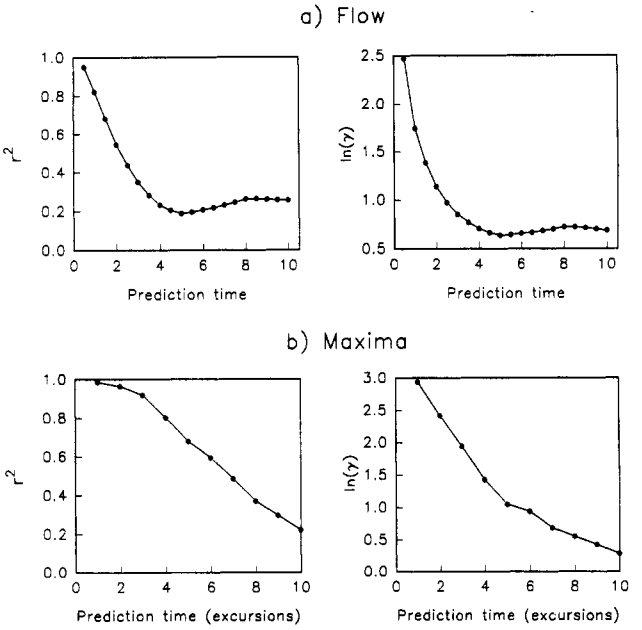

Figure 13. Nonlinear forecasting of (a) time series and (b) maxima obtained from the Olsen 83 model. In (a) 10 000 data of A were embedded in 3 dimensions using a time delay, T = 1. The first 5000 points were used as an "atlas" to predict the remaining 5000 points. In each prediction only the points within an epsilon ball corresponding to 2% of the maximum signal size were used for the prediction and the maximum number of such points were furthermore limited to 5. In (b) 500 maxima were embedded in 2 dimensions using a time delay, T = 1 excursion. The first 250 maxima were used as an atlas to predict the remaining 250 maxima. In each prediction only the nearest 3 points were used. $k_3 = 3.5 \times 10^{-2}$. Other rate constants as in Figure 10.

corresponding values of D_L, except for values of $k_3 < 0.034$ where the dynamics correspond to periodic oscillations. This is to be expected, since, as noted above, $D_2 < D_L$[21,60] for nonuniform data.

Comparison of Tables I and III reveals that the estimates of λ_1 and D_2 obtained from chaos in the Olsen 83 model are smaller than those obtained from the experimental data. In this regard, one must bear in mind that the experimental time series are subject to two additional factors: In the first place, it is presently not possible to obtain the large number of maxima needed to accurately estimate the maximum exponent. Fifty to 100 post-transient oscillations are all that can be presently managed. As shown in Table IV, time series of this length overestimate λ_1 by a factor of about 50%. To a lesser degree, short time series also overestimate D_2. In addition, the experimental data are subject to dynamical noise in the form of random perturbations. In particular, the very low pumping rate of NADH into the reaction chamber (on the order of μL/h) makes it inevitable that there will be small random variations in the rate of infusion of this substance.[70] To study the effects of these variations, we generated additional solutions to the model, this time with small amounts of noise added to the variable B.[70] Figure 12 shows plots of ln ($C(g)$) *vs* ln (g) and next-amplitude maps for increasing amounts of noise. With increasing noise, the log–log plots become biphasic. At length scales corresponding to the noise level the slope increases almost linearly with the embedding dimension. If the noise amplitude is small, the slope saturates with increasing embedding dimension at intermediate length scales. At higher noise levels the scaling region disappears and the slope continues to increase with the embedding dimension. The corresponding estimates of D_2 are listed in Table V. Comparison with Table III indicates an insignificant increase in D_2 for σ = 0.005. Table V also gives estimates of the maximum LCE in the presence of noise. The resulting values are somewhat lower than the corresponding estimate for the noise-free system (Table III) and essentially independent of the noise level. In sum, dynamical noise in the form of random perturbations to the influx of NADH is more likely to compromise one's ability to estimate D_2 than λ_1.

Finally, we subjected both the continuous time series, $\{A(t)\}$ and the next-amplitude maps to nonlinear forecasting. The results are summarized in Figure 13. For the time series (Figure 13a), r^2 declines rapidly with the prediction interval, the situation being comparable to what one observes in experimental data; *i.e.*, we are unable to generate accurate predictions over a time scale corresponding to the average period of oscillation which here corresponds to 11.7 time units. Moreover, the plot of ln (γ) *versus* prediction interval is nonlinear, and from the first few prediction steps we estimate a maximum Lyapunov exponent of more than 20 bits/excursion. This is twice as high as the corresponding exponent computed from the experimental time series. Repeating the procedure for the next-amplitude maps

results in a much slower decline in r^2 and a plot of ln (γ) *versus* prediction time which is linear up to five excursions. From the latter we estimate $\lambda_1 = 0.72$ bit/excursion, which is more nearly in agreement with the values computed directly from the differential equations or from the series of maxima ($\lambda_1 = 0.44$ bit/excursion) using the algorithms in ref 13. In sum, the Olsen 83 model is even more nonuniform than the experimental data.

4.2. Model C. Aguda and Larter[68] have proposed the following detailed model of the peroxidase oxidase reaction:

$$\mathrm{Per^{3+}} + \mathrm{H_2O_2} \xrightarrow{k_1} \mathrm{coI}$$

$$\mathrm{coI} + \mathrm{NADH} \xrightarrow{k_2} \mathrm{coII} + \mathrm{NAD^{\bullet}} + \mathrm{H^+}$$

$$\mathrm{coII} + \mathrm{NADH} \xrightarrow{k_3} \mathrm{Per^{3+}} + \mathrm{NAD^{\bullet}} + \mathrm{H^+}$$

$$\mathrm{coIII} + \mathrm{NAD^{\bullet}} \xrightarrow{k_4} \mathrm{coI} + \mathrm{NAD^+}$$

$$\mathrm{Per^{3+}} + \mathrm{O_2^-} \xrightarrow{k_5} \mathrm{coIII}$$

$$\mathrm{NAD^{\bullet}} + \mathrm{O_2} \xrightarrow{k_6} \mathrm{NAD^+} + \mathrm{O_2^-}$$

$$\mathrm{H^+} + \mathrm{O_2^-} + \mathrm{NADH} \xrightarrow{k_7} \mathrm{H_2O_2} + \mathrm{NAD^{\bullet}}$$

$$2\mathrm{NAD^{\bullet}} \xrightarrow{k_8} (\mathrm{NAD})_2$$

$$\xrightarrow{k_9} \mathrm{O_2}$$

$$\mathrm{O_2} \xrightarrow{k_{10}}$$

$$\xrightarrow{k_{11}} \mathrm{NADH}$$

$$\mathrm{Per^{3+}} + \mathrm{NAD^{\bullet}} \xrightarrow{k_{12}} \mathrm{Per^{2+}} + \mathrm{NAD^+}$$

$$\mathrm{Per^{2+}} + \mathrm{O_2} \xrightarrow{k_{13}} \mathrm{coIII}$$

where Per^{2+} and Per^{3+} denote ferrous peroxidase and ferric peroxidase, respectively; coI, coII, and coIII denote compound I, compound II, and compound III; $NAD^{\bullet}$ is the free radical obtained by removing a hydrogen atom from NADH and O_2^- is the superoxide radical. Reactions 9 and 10 represent the diffusion of O_2 into the reaction mixture across the gas/liquid interface, and reaction 11 represents the constant rate of infusion of NADH.

Model C translates into 10 differential equations, which can be brought into the following dimensionless form:

$$\epsilon_a \frac{da}{d\tau} = cn - aw \tag{17}$$

$$\epsilon_b \frac{db}{d\tau} = (c + x + y)n - (f + w + z)b - 2\gamma b^2 \tag{18}$$

$$\epsilon_c \frac{dc}{d\tau} = bf - (n + w)c \tag{19}$$

$$\frac{df}{d\tau} = 1 - (1 + b + v)f \tag{20}$$

$$\epsilon_n \frac{dn}{d\tau} = \alpha - (c + x + y)n \tag{21}$$

$$\epsilon_w \frac{dw}{d\tau} = yn - (a + b + c)w \tag{22}$$

$$\epsilon_x \frac{dx}{d\tau} = bz + aw - xn \tag{23}$$

$$\epsilon_y \frac{dy}{d\tau} = (x - y)n \tag{24}$$

$$\epsilon_z \frac{dz}{d\tau} = cw + vf - bz \tag{25}$$

$$\epsilon_v \frac{dv}{d\tau} = bw - vf \tag{26}$$

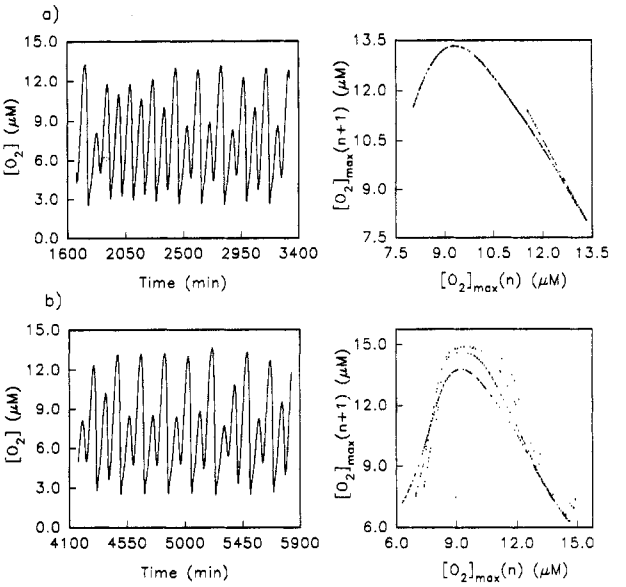

Figure 14. Time series (left panel) and next-amplitude maps (right panel) of two aperiodic oscillations of O_2 obtained from model C. The rate constants used in both simulations were $k_1 = k_2 = k_3 = k_4 = k_6 = k_7 = k_8 = k_{12} = k_{13} = 2.67 \times 10^3$ M^{-1} s^{-1}, $k_5 = 1.6 \times 10^5$ M^{-1} s^{-1}, $k_9 = 6.0 \times 10^{-8}$ M s^{-1}, $k_{10} = 4.0 \times 10^{-3}$ s^{-1}, $k_{11} = 6.0 \times 10^{-8}$ M s^{-1}. The following initial conditions were $[H_2O_2] = 1.90 \times 10^{-9}$ M, $[NAD] = 4.76 \times 10^{-7}$ M, $[O_2^-] = 7.26 \times 10^{-9}$ M, $[O_2] = 1.137 \times 10^{-5}$ M, $[NADH] = 3.13 \times 10^{-5}$ M, $[Per^{3+}] = 1.14 \times 10^{-5}$ M, [coI] = [coII] = 3.0×10^{-7} M, [coIII] = 1.8×10^{-5} and (a) $[Per^{2+}] = 3.0 \times 10^{-5}$ M or (b) $[Per^{2+}] = 3.1 \times 10^{-5}$ M. This means that in (a) the total enzyme concentration is 6.0×10^{-5} M whereas in (b) it is 6.1×10^{-5} M.

The dimensionless variables and the scaling coefficients are defined as follows:

$$\tau = k_{10}t; \quad a = \frac{k_1 k_6 [\mathrm{H_2O_2}]}{k_{10} k_{12}}; \quad b = \frac{k_6 [\mathrm{NAD^{\bullet}}]}{k_{10}};$$

$$c = \frac{k_5 k_6 [\mathrm{O_2^-}]}{k_{10} k_{12}}; \quad f = \frac{k_{10} [\mathrm{O_2}]}{k_9}; \quad n = \frac{k_7 k_{10} k_{12} [\mathrm{NADH}]}{k_5 k_6 k_9};$$

$$w = \frac{k_{10} k_{12} [\mathrm{Per^{3+}}]}{k_6 k_9}; \quad x = \frac{k_2 k_5 k_6 [\mathrm{coI}]}{k_7 k_{10} k_{12}}; \quad y = \frac{k_3 k_5 k_6 [\mathrm{coII}]}{k_7 k_{10} k_{12}};$$

$$z = \frac{k_4 k_{10} [\mathrm{coIII}]}{k_6 k_9}; \quad v = \frac{k_{13} [\mathrm{Per^{2+}}]}{k_{10}}; \quad \alpha = \frac{k_{11}}{k_9};$$

$$\epsilon_a = \frac{k_{10}^2 k_{12}}{k_1 k_6 k_9}; \quad \epsilon_b = \frac{k_{10}^2}{k_6 k_9}; \quad \epsilon_c = \frac{k_{10}^2 k_{12}}{k_5 k_6 k_9}; \quad \epsilon_n = \frac{k_5 k_6}{k_7 k_{12}};$$

$$\epsilon_x = \frac{k_7 k_{10}^2 k_{12}}{k_2 k_5 k_6 k_9}; \quad \epsilon_y = \frac{k_7 k_{10}^2 k_{12}}{k_3 k_5 k_6 k_9}; \quad \epsilon_v = \frac{k_{10}^2}{k_9 k_{13}}; \quad \epsilon_w = \frac{k_6}{k_{12}};$$

$$\epsilon_z = \frac{k_6}{k_4}; \quad \gamma = \frac{k_8 k_{10}^2}{k_9 k_6^2}$$

The parameters used in simulating model C were the same as those used by Aguda and Larter:[68] $\epsilon_a = \epsilon_b = \epsilon_v = \gamma = 0.1$; $\epsilon_w = \epsilon_z = \alpha = 1.0$; $\epsilon_c = \epsilon_x = \epsilon_y = 0.001\,67$; and $\epsilon_n = 60$. From these parameters and the rate constants k_9, k_{10}, and k_{11}, one can estimate the rate constants k_1–k_8, k_{12}, and k_{13}.

Dichlorophenol and methylene blue are not included in model C and hence we cannot explore the consequences of changing its concentration. However, model C is able to reproduce the transition from periodic oscillation to chaos by decreasing the enzyme concentration as observed in previous experiments.[5] Figure 14 shows two examples of apparently chaotic oscillations induced by the model. Time series of $[O_2]$ are displayed at the left and next-amplitude maps at the right. The latter bear a greater degree

TABLE VI: Maximum Lyapunov Exponents and Correlation Dimensions Computed for the Flows of [O_2] and the Corresponding Maxima for Two Simulations of Model C at Two Different Enzyme Concentrations[a]

	flow		maxima	
$[E]_t$, M	λ_1, bit/excursion	D_2	λ_1, bit/excursion	D_2
6.0×10^{-5}	0.54	2.17	0.49	1.01
6.1×10^{-5}	0.95	2.03	0.81	1.13

[a] 10 000 continuous data sampled at Δt = 50 s or approximately 350 maxima were used in the calculations.

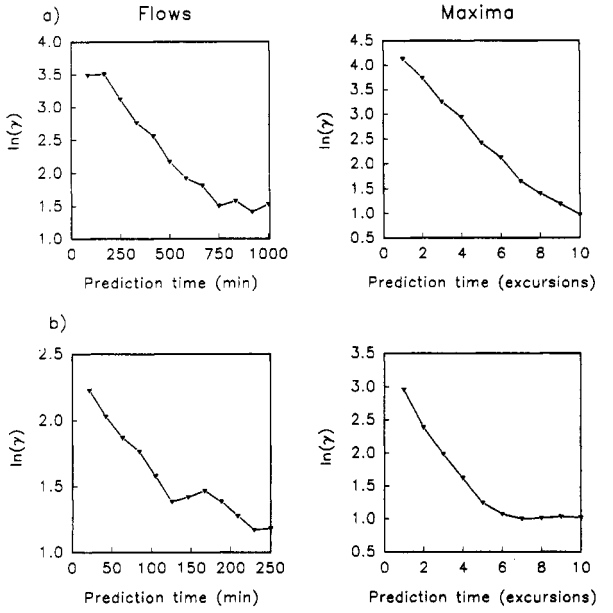

Figure 15. Nonlinear forecasting of chaotic time series and maxima generated by model C. In (a) 10 000 data of O_2 were embedded in 3 dimensions using a time delay, T = 500 s. The first 5000 points were used as an "atlas" to predict the remaining 5000 points. In each prediction only the points within an epsilon ball corresponding to 2% of the maximum signal size were used for the prediction and the maximum number of such points were furthermore limited to 5. In (b) 350 maxima were embedded in 2 dimensions using a time delay, T = 1 excursion. The first 175 maxima were used as an atlas to predict the remaining 175 maxima. In each prediction only the nearest 3 points were used. Parameters as in Figure 14.

of similarity to those obtained experimentally (Figure 3) than corresponding maps obtained from the Olsen 83 model (Figure 11).

Maximum Lyapunov exponents and the correlation dimension were obtained from simulated time series of [O_2] generated by model C. The results of these computations are summarized in Table VI. Note that there is good correspondence between the values of λ_1 and D_2 computed from the time series and sequences of successive maxima. This indicates that the model C's output is more uniform than the experimental data as well as the time series induced by the Olsen 83 model. In order to investigate this further we subjected the time series and the next-amplitude maps to nonlinear forecasting, the results of which are summarized in Figure 15. Here we plot ln (γ) *versus* the prediction interval. In this regard, we note first that the flows are much more predictable than those from the experiments and the Olsen 83 model. The average period of the oscillations corresponding to Figure 15a was 87.9 min, whereas that corresponding to Figure 15b was 98.5 min. From the initial slopes of the plots in Figure 15 we compute maximum Lyapunov exponents of 0.58 bit/excursion and 0.56 bit/excursion for the flows and maxima, respectively, at $[E]_t = 6 \times 10^{-5}$ M (Figure 15a) and 0.98 bit/excursion and 0.58 bit/excursion, respectively, at $[E]_t = 6.1 \times 10^{-5}$ M (Figure 15b). Since the values computed from the flows and next amplitudes are in general the same, these results may be taken as further evidence that the data generated by model C are fairly uniform compared to the experimental data and the data generated by the Olsen 83 model.

5. Conclusion

From the nonlinear analyses of the experimental data we draw the following conclusions:

1. The observation of period doubling bifurcations leading to aperiodic oscillations and well-defined next-amplitude maps of the latter, provide convincing evidence for chaos in the experimental system.

2. The data are nonuniform since attempts to compute maximum Lyapunov exponents and correlation dimensions directly from the aperiodic time series fail to give meaningful values.[21,60] However, reasonable estimates of these quantities can be made from a series of maxima (Poincaré section), with as little as 50–100 data points.

3. The problems associated with the nonuniformity of the data are also encountered when subjecting the time series to nonlinear forecasting algorithms. Here, we find that predictability declines rapidly and is essentially gone at prediction times corresponding to the length of an average period. However, if we use the series of maxima instead, predictability may be extended to several periods. The Lyapunov exponents computed from these latter predictability profiles are in good agreement with the exponents computed using other methods.

Repeating the procedures discussed above using data generated by a simple model of the reaction yield similar results: Reliable estimates of λ_1 and D_2 cannot be obtained using a continuous time series, irrespective of the number of data points. However, Lyapunov exponents and dimensions can be computed from a series of maxima. The values of D_2 are typically smaller than the corresponding Lyapunov dimensions. Failure to compute λ_1 and D_2 directly from continuous aperiodic time series and a significant difference between D_2 and D_L suggest that the chaotic data from the model are also nonuniform. We further investigated the effects of varying the number of data points and of adding random perturbations to the simulations, and found that reliable estimates of D_2 can be made with as few as 50–100 maxima and in the presence of low levels of external noise. High levels of noise prohibit estimates of D_2 due to a decrease in the scaling region and a lack of saturation of slope with increasing embedding dimension. The maximum Lyapunov exponent can also be computed for 50 maxima of oscillations and the exponent is relatively unaffected by noise. The Lyapunov exponents obtained from the model data were similar to those obtained from the experimental data using the same number of maxima, but the correlation dimensions were generally lower than those obtained with the experimental data. However, the latter may be due to the existence of noise in the experimental system and lack of a sufficient amount of data. Furthermore, for the simulations we observe a similar rapid decline in predictability with prediction time when using a continuous time series, as opposed to a series of maxima. However, the model data differ from the experimental data in that the next-amplitude maps are clearly different, and the former are even more nonuniform than the latter, as suggested by the more rapid decline in predictability with prediction time observed for the model data.

The corresponding analyses of a detailed model (model C) reveal next-amplitude maps with a striking similarity to the maps obtained from the experimental data. Furthermore, the maximum Lyapunov exponents and correlation dimensions estimated from the model data are similar to those computed for the experimental data. However, the data generated by this model are essentially uniform, since we obtain almost the same Lyapunov exponents and correlation dimensions from a continuous time series and the corresponding series of maxima, and the predictability of the continuous data and the maxima are the same over comparable

time scales. Furthermore, the parameters proposed by Aguda and Larter[68] are unrealistic in that they yield periods of oscillation which are about 50–100 times longer that the periods observed in the experiments and they predict enzyme concentrations at which chaos is observed which are 2 orders of magnitude higher than those used in the experiments. However, a recent study suggests that periodic and chaotic oscillations with periods closer to the experiments can be obtained from model C, using more realistic parameters and enzyme concentrations.[71]

Thus, from comparing experimental and numerical data we conclude that none of the models discussed here can describe the data adequately. However, the minimal (Olsen 83) model qualifies as the best model, because, in addition to yielding similar characteristic measures, it also reproduces the nonuniformity of the data. Hence, we conclude that the chaotic attractor in the peroxidase–oxidase reaction is nonuniform and has a maximum Lyapunov exponent corresponding to about 0.5 bit/excursion and a fractal dimension between 2 and 3. The fractal dimension obtained here is similar to that obtained for other chemical and biochemical systems with chaotic behavior.[38,72,73]

Acknowledgment. This work was supported by grants from the Danish Natural Science Research Council, National Institute of Health, NATO Scientific Affairs Division, and the Natural Science Faculty, Odense University. We are grateful to Lars Teil Nielsen, Thomas Graf, and Tommy Nørnberg for help with the experimental setup.

References and Notes

(1) Olsen, L. F.; Degn, H. *Q. Rev. Biophys.* **1985**, *18*, 165.
(2) Schaffer, W. M. *IMA J. Math. Appl. Med. Biol.* **1985**, *2*, 221.
(3) Holden, A. V. *Chaos*; Manchester University Press: Manchester, U.K., 1986.
(4) Degn, H., Holden, A. V., Olsen, L. F., Eds. *Chaos in Biological Systems*; NATO ASI Series, Series A, Life Sciences; Plenum Press: New York, 1987; Vol. 138.
(5) Olsen, L. F.; Degn, H. *Nature* **1977**, *267*, 177.
(6) Markus, M.; Kuschmitz, D.; Hess, B. *FEBS Lett.* **1984**, *172*, 235.
(7) Glass, L.; Mackey, M. C. *From Clocks to Chaos, The Rhythms of Life*; Princeton University Press: Princeton, NJ, 1988.
(8) Babloyantz, A.; Destexhe, A. *Proc. Natl. Acad. Sci. USA* **1986**, *83*, 3513.
(9) Goldberger, A. L.; Rigney, D.; West, B. J. *Sci. Am.* **1990**, February 35.
(10) Allen, J. C.; Schaffer, W. M.; Rosko, D. *Nature*, in press.
(11) Ruelle, D. *Ann. N.Y. Acad. Sci.* **1979**, *316*, 408.
(12) Bennetin, G.; Galgani, L.; Giorgilli, A.; Strelcyn, J.-M. *Meccanica* **1980**, *15*, 9.
(13) Wolf, A.; Swift, J. B.; Swinney, H. L.; Vastano, J. *Physica D* **1985**, *16*, 285.
(14) Eckmann, J.-P.; Ruelle, D. *Rev. Mod. Phys.* **1985**, *57*, 617.
(15) Ford, J. *Physics Today* **1983**, *April*, 40.
(16) Degn, H. *Phys. Rev. A* **1983**, *26*, 711.
(17) Farmer, D.; Crutchfield, J.; Froehling, H.; Packard, N.; Shaw, R. *Ann. N.Y. Acad. Sci.* **1980**, *357*, 453.
(18) Farmer, J. D.; Ott, E.; Yorke, J. A. *Physica D* **1983**, *7*, 153.
(19) Grebogi, C.; Ott, E.; Pelikan, S.; Yorke, J. A. *Physica D*, **1984**, *13*, 261.
(20) Nicolis, J. S.; Mayer-Kress, G.; Haubs, G. *Z. Naturforsch.* **1983**, *36a*, 1157.
(21) Ebling, W.; Herzel, H.; Schimansky-Geier, L. In *From Chemical to Biological Organization*; Markus, M., Müller, S. C., Nicolis, G., Eds.; Springer-Verlag: Berlin, 1988; p 166.
(22) May, R. M. *Nature* **1978**, *278*, 505.
(23) Scott, S. K. Chemical Chaos. *International Series of Monographs on Chemistry*; Clarendon Press: Oxford, U.K., 1991; Vol. 24.
(24) May, R. M. *Nature* **1976**, *261*, 459.
(25) Feigenbaum, M. J. *J. Stat. Phys.* **1978**, *19*, 25–52.
(26) Yamazaki, I.; Yokota, K.; Nakajima, R. *Biochem. Biophys. Res. Commun.* **1965**, *21*, 582.
(27) Nakamura, S.; Yokota, K.; Yamazaki, I. *Nature* **1969**, *222*, 794.
(28) Olsen, L. F.; Degn, H. *Biochim. Biophys. Acta* **1978**, *523*, 321.
(29) Fed'kina, V. R.; Bronnikova, T. V.; Ataullakhanov, F. I. *Stud. Biophys* **1981**, *82*, 159.
(30) Olsen, L. F. *Phys. Lett. A* **1983**, *94*, 454.
(31) Olsen, L. F. In *Stochastic Phenomena and Chaotic Behavior in Complex Systems*; Schuster, P., Ed., Springer-Verlag: Berlin, 1984; p 116.
(32) Geest, T.; Steinmetz, C. G.; Larter, R.; Olsen, L. F. *J. Phys. Chem.* **1992**, *96*, 5678.
(33) Rys, P.; Wang, J. *Biochem. Biophys. Res. Commun.* **1992**, *186*, 612.
(34) Samples, M.; Hung, Y.-F.; Ross, J. *J. Phys. Chem.* **1992**, *96*, 7338.
(35) Hauck, T.; Schneider, F. W. *J. Phys. Chem.* **1993**, *97*, 391.
(36) Degn, H.; Lundsgaard, J.; Petersen, L. C.; Ormicky, A. In *Methods of Biochemical Analysis*; Glick, D., Ed.; Wiley & Sons: New York, 1979; Vol. 26, p 47.
(37) Takens, F. *Lect. Notes Math.* **1981**, *898*, 366.
(38) Roux, J.-C.; Simoyi, R. H.; Swinney, H. L. *Physica* **1983**, *8D*, 257.
(39) Schaffer, W. M.; Kot, M. *J. Theor. Biol.* **1985**, *112*, 403.
(40) Historically, this procedure was utilized both in mathematical models (refs 41 and 42) and the peroxidase system itself (ref 5), before the discovery of state space reconstruction techniques.
(41) Lorenz, E. N. *J. Atmos. Sci.* **1963**, *20*, 130.
(42) Rössler, O. E. *Z. Naturforsch.* **1976**, *31a*, 259.
(43) Grassberger, P.; Procaccia, I. *Physica D* **1983**, *9*, 189.
(44) Farmer, J. D.; Sidorowich, J. *Phys. Rev. Lett.* **1987**, *59*, 845.
(45) Sugihara, G.; May, R. M. *Nature* **1990**, *344*, 734.
(46) Farmer, J. D.; Sidorowich, J. J. In *Dynamic Patterns in Complex Systems*; Kelso, J. A. S.; Mandell, A. J., Shlesinger, M. F., Eds.; World Scientific: Singapore, 1988; p 265.
(47) Wales, D. J. *Nature* **1991**, *350*, 485.
(48) Osborne, A. R.; Provenzale, A. *Physica D* **1989**, *35*, 357.
(49) Ruelle, D. *Proc. R. Soc. London A* **1990**, *427*, 241.
(50) Other authors have used higher order local maps (ref 51). Still others advocate the use of global predictors (ref 52), in which case, one induces a single equation from the data in the atlas, and finally, there are the proponents of neural networks (ref 53). Of course, there is considerable disagreement (ref 54) as to the relative merits of different predictors, a fact which is hardly surprising given both the newness of the approach and the variable nature of chaotic time series.
(51) Farmer, J. D.; Sidorowich, J. J. In *Evolution, Learning and Cognition*; Lee, Y. C., Ed.; World Scientific: Singapore, 1988; p 277.
(52) Cremers, J.; Hübler, A. *Z. Naturforsch.* **1987**, *42a*, 797.
(53) Lapedes, A.; Farber, R. *Tecnical Report LA-UR-87-2662*; Los Alamos National Laboratory, Los Alamos, 1987.
(54) Casdagli, M. *Physica D* **1989**, *35*, 335.
(55) Schaffer, W. M.; Tidd, C. W. *NLF: Nonlinear Forecasting for Chaotic Dynamical Systems*. Dynamical Systems, Inc.: Tucson, AZ, 1990.
(56) Note that for small length scales, the curves steepen due to noise in the data (ref 57).
(57) Ben-Mizrachi, A.; Procaccia, I.; Grassberger, P. *Phys. Rev. A* **1984**, *29*, 975.
(58) This is a consequence of the fundamental uniqueness property of differential equations, *i.e.*, a dimension of 2 or less would necessitate self-intersecting trajectories.
(59) Albano, A. M.; Mees, A. I.; de Guzman, C. G.; Rapp, P. E. In *Chaos in Biological Systems*; Degn, H., Holden, A. V., Olsen, L. F., Eds.; Plenum Press: New York, 1987; p 207.
(60) Schaffer, W. M.; Olsen, L. F.; Truty, G. L.; Fulmer, S. L.; Graser, D. J. In *From Chemical to Biological Organization*; Markus, M., Müller, S. C., Nicolis, G., Eds.; Springer-Verlag: Berlin, 1988; p 331.
(61) Shaw, R. *Z. Naturforsch.* **1981**, *36a*, 80.
(62) Tidd, C. W.; Schaffer, W. M., Olsen, L. F. *Proc. R. Soc. London B*, submitted for publication.
(63) The fact that chaotic time series can evidence significant periodicity as measured, for example, by the power spectrum is discussed in ref 17. A good example is the Rössler attractor (ref 64) which evidences spectral peaks that are instrumentally sharp. In fact the observation of statistical periodicity in chaotic data is no accident. Chaotic attractors are organized around what have been called "skeletons" of nonstable periodic orbits. Sometimes these orbits are dense on the attractor (ref 65).
(64) Rössler, O. E. *Phys. Lett. A* **1976**, *35*, 397.
(65) Kirchgraber, U.; Stoffer, D. *SIAM Rev.* **1990**, *32*, 424.
(66) Fed'kina, V. R.; Ataullakhanov, F. I.; Bronnikova, T. V. *Biophys. Chem.* **1984**, *19*, 259.
(67) Aguda, B. D.; Larter, R. *J. Am. Chem. Soc.* **1990**, *112*, 2167.
(68) Aguda, B. D.; Larter, R. *J. Am. Chem. Soc.* **1991**, *113*, 7913.
(69) Steinmetz, C. G.; Geest, T.; Larter, R. *J. Phys. Chem.* **1993**, *97*, 5649.
(70) Olsen, L. F. *Z. Naturforsch.* **1985**, *36a*, 80.
(71) Klein, M. M.S. Thesis, Indiana University–Purdue University at Indianapolis, Indianapolis, 1992.
(72) Wicke, E.; Onken, H. U. In *From Chemical to Biological Organization*; Markus, M., Müller, S. C., Nicolis, G., Eds.; Springer-Verlag: Berlin, 1988, p 62.
(73) Markus, M.; Hess, B. In *Temporal Order*; Rensing, L., Jaeger, N. I., Eds.; Springer-Verlag: Berlin, 1985; p 191.